Eur. Phys. J. A **22**, 69–74 (2004)
DOI 10.1140/epja/i2003-10231-y

THE EUROPEAN PHYSICAL JOURNAL A

Changes in the mean square charge radii of neutron-deficient europium isotopes measured by the laser ion source resonance ionization spectroscopy

A.E. Barzakh, D.V. Fedorov[1,a], A.M. Ionan, V.S. Ivanov, F.V. Moroz, K.A. Mezilev, S.Yu. Orlov, V.N. Panteleev, and Yu.M. Volkov

Petersburg Nuclear Physics Institute RAS (PNPI), 188300 Gatchina, Leningrad district, Russia

Received: 10 November 2003 / Revised version: 28 April 2004 /
Published online: 19 October 2004 –
Communicated by J. Äystö

Abstract. The laser ion source has been used for the study of the isotope shifts of neutron-deficient Eu isotopes. The extension of the region of applicability of the method by using the γ- and β-radiation detection is reported. We have measured the isotope shifts of the europium optical line 576.520 nm for $^{137-139,141,142m,143,144}$Eu. To increase the laser ion source efficiency an axial magnetic field (350 gauss) was applied. Nearly a twofold rise of the ionization efficiency for Eu was observed. By using the effect of optical ion bunching an increase of the selectivity was obtained. The isotope shift data for ^{139,141,142m,143,144}Eu are in agreement with the previously measured isotope shifts for these nuclides. The new data for ^{137}Eu and refined data for ^{138}Eu point to a gradual increase of the deformation for these isotopes. Comparisons with microscopic-macroscopic calculations and calculations in the framework of the Hartree-Fock model were performed.

PACS. 29.25.Rm Sources of radioactive nuclei – 42.62.Fi Laser spectroscopy – 21.10.-k Properties of nuclei; nuclear energy levels – 21.10.Ft Charge distribution

1 Introduction

Investigations of the ground-state properties of the europium radioactive isotopes have attracted much attention for a long time [1–3]. Isotope shift measurements of the long isotopic chain are of special interest in order to study the nuclear shape transition from spherical ($N = 82$) to strongly deformed nuclei at neutron numbers $N = 88$, 89 and the deformation behaviour at $N < 82$. The course of changes in mean square charge radii extracted from the isotope shifts reflects the isotopic change of nuclear deformation.

Laser spectroscopy techniques provide an excellent tool for optical isotope shift measurements. High sensitivity and resolution allow one to investigate long chains of short-lived isotopes [3–5]. In this article recent developments of the laser ion source spectroscopy technique and the results of isotope shift measurements on very neutron-deficient Eu are presented.

[a] e-mail: dfedorov@pnpi.spb.ru

2 Experimental method

2.1 Outline of the basics of the laser ion source resonance ionization method

The method of resonance laser photoionization in the laser ion source proves to be one of the most efficient tools for isotope shift and hyperfine-structure investigations [5,6]. The essential point of the experimental method is the step-by-step resonant laser excitation to autoionization states or the continuum. To extend the investigations of isotope shifts and hyperfine structure to the more neutron-deficient isotopes, first of all to the region of neutron-deficient isotopes near and below the magic neutron number $N = 82$, the method of photoionization spectroscopy inside the laser ion source has been proposed and applied at the IRIS facility [5,6].

The experimental set-up is presented in fig. 1. The nuclides under study are produced in the target of the mass separator by 1 GeV protons of the PNPI synchrocyclotron. The atoms are thermally released from the target to the ion source cavity (tungsten tube with a length of 50 mm

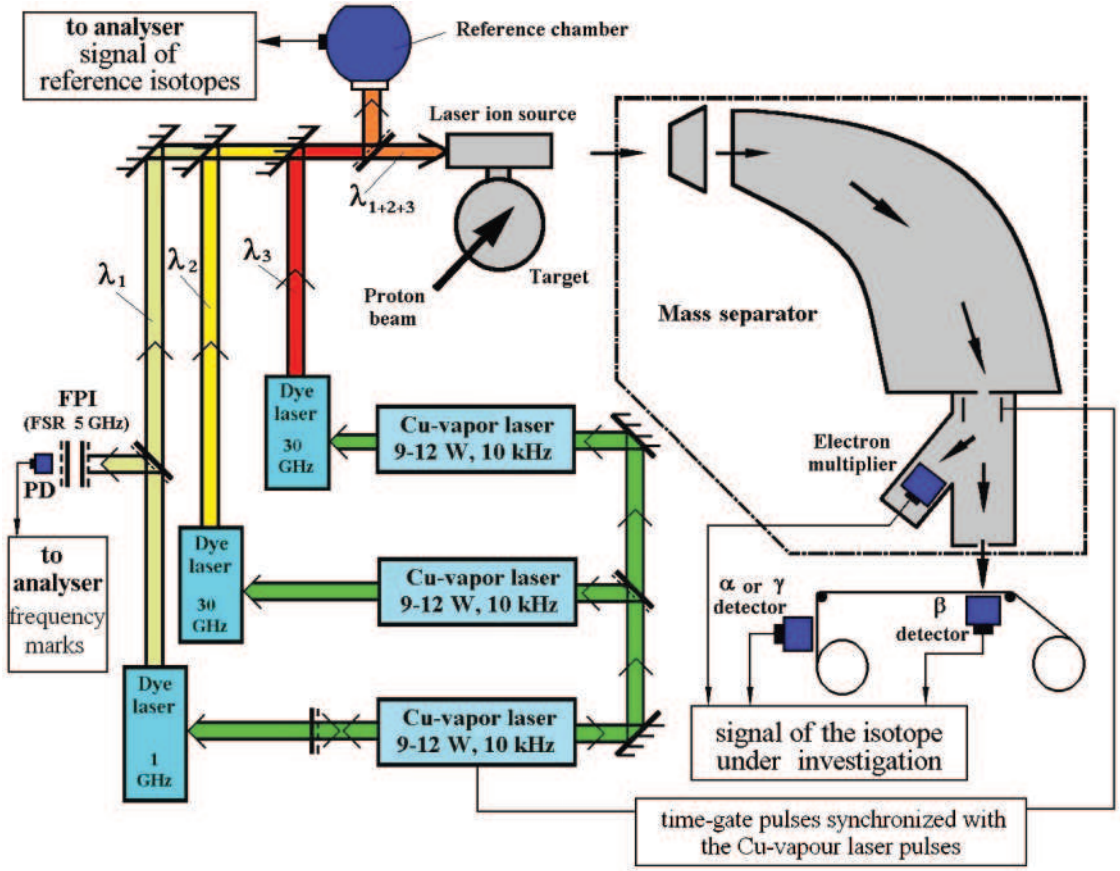

Fig. 1. Experimental set-up. FPI: Fabry-Perot interferometer, PD: photodiode.

and 1 mm in diameter). Three beams from pulsed dye lasers are introduced to the same cavity to provide multi-step resonance ionization of the atoms under investigation.

The dye lasers are pumped by three copper vapour lasers (repetition rate 10 kHz). The wavelengths of the dye lasers are tuned to the transitions of the chosen ionization scheme. The radiation frequency of the two broad-band lasers (bandwidth 30 GHz) is fixed to the wavelengths of the second and the third transition (557.27 nm and 555.70 nm). The wavelength of the narrow-band laser (bandwidth 1 GHz) is scanned across the first transition (576.52 nm). The photoion current in the collector of the mass separator increases at the resonance. Thus, the experimental spectra represent the dependence of the ion current on the scanned laser frequency. The detection of ion current is provided by alpha-, beta-, or gamma-counting. These detectors are installed at a tape system.

A part of the scanning laser radiation is directed to the Fabry-Perot interferometer (FPI) (free spectral range (FSR) 5 GHz) to produce the frequency marks for frequency calibration. Another part of the laser beam is used in a reference chamber to provide a reference spectrum from the sample of stable isotopes for the isotope shifts measurements. An example of the experimental spectra is presented in fig. 2.

Due to the thermal motion of the atoms inside the laser ion source cavity, Doppler broadening of the resonance line takes place. This limits the resolution of the experimental method to 1.5 GHz for heavy atoms. The hyperfine splitting of the transition used for isotope shifts measurements (576.52 nm) is anomalously small (less than 300 MHz for ^{151}Eu) [7]. As was checked by simulations, this hyperfine splitting does not affect the centre of gravity of the observed line in cases where the line width is greater than 1.0 GHz.

The efficiency of laser ionization was as high as 10% for stable ^{153}Eu as checked in the off-line measurements. The high efficiency of the method is explained by the following factors [8]:

1) the multiple interaction of the laser beam with the atom during the residence time of the atoms inside the laser ion source considerably increases the probability of photoionization;

2) the electron emission from the hot inner surface of the ion source creates an electric potential near the cavity wall which traps photoions near the central axis and prevents their recombination on the wall surface.

On-line experiments with neutron-deficient Yb, Tm [6] and Eu isotopes (present work) have demonstrated the very high sensitivity of the method. The minimal production rate, sufficient for isotope shift measurements with the laser ion source, is about 10–100 nuclides per second.

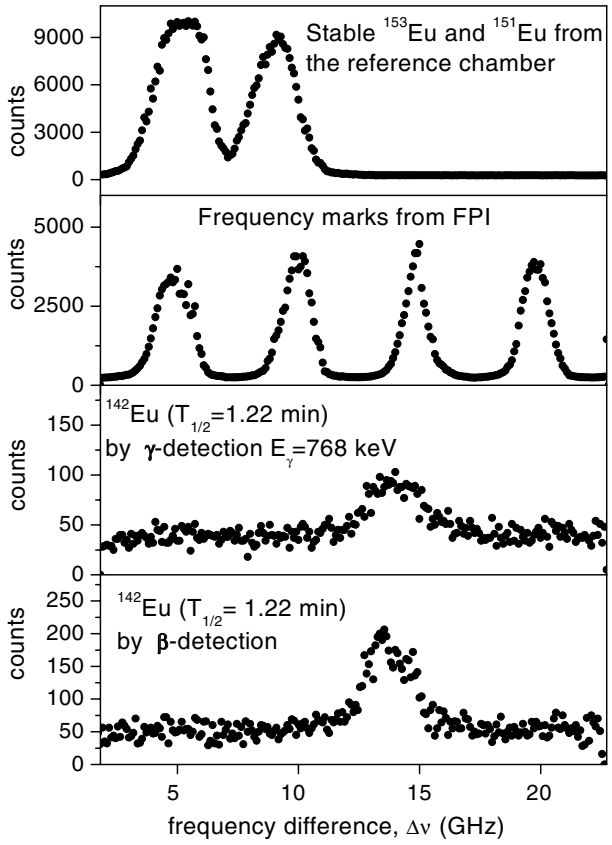

Fig. 2. Example of the experimental spectra.

2.2 New developments for efficiency and selectivity improvement

2.2.1 Axial-magnetic-field application for the efficiency rise

The positive effect of an axial magnetic field in a high-temperature electron beam ion source has been demonstrated earlier [9]. It enhances the ionization efficiency of atoms with high ionization potentials such as W, Ta, Sn. It was explained by the trapping of ionized atoms in an electron beam compressed by the applied axial magnetic field. A similar increase of the ion currents for elements with considerably lower potentials of ionization (In, Gd, Tm, Yb, Lu, etc.) has been also observed [10]. This effect is assumed to be caused by the confinement of the ions in the thermoelectron beam produced in the cavity by the heating voltage drop and by the magnetic field. Due to this confinement, ions are prevented from recombination on the wall of the ion source. A strong influence of the magnetic field on the ionization efficiency was shown in on-line experiments [10]. For radioactive neutron-rich In isotopes the ionization efficiency rises by a factor of 4.5.

The observed magnetic-field effect was used to raise the ionization efficiency of the laser ion source in on-line experiments with neutron-deficient Eu isotopes. Figure 3 presents a schematic drawing of the laser ion source of the high-temperature target unit.

Off-line tests have demonstrated the increase of the ^{153}Eu photoion current when an axial magnet field up to

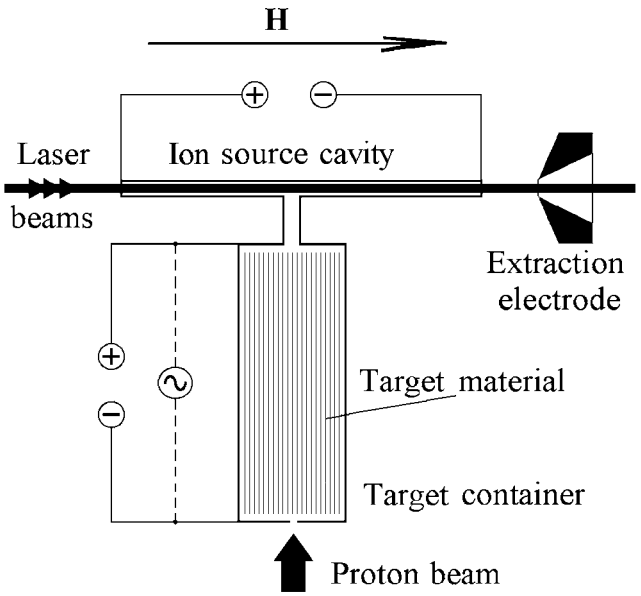

Fig. 3. Schematic drawing of the laser ion source in combination with the high-temperature target unit.

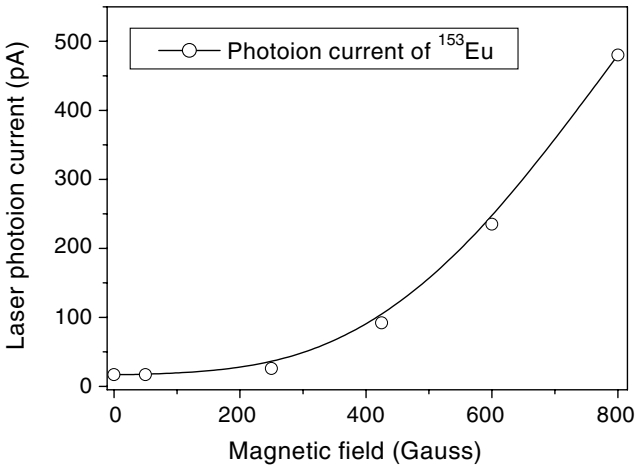

Fig. 4. Dependence of the ^{153}Eu photoion current on the axial magnetic field applied to the ion source.

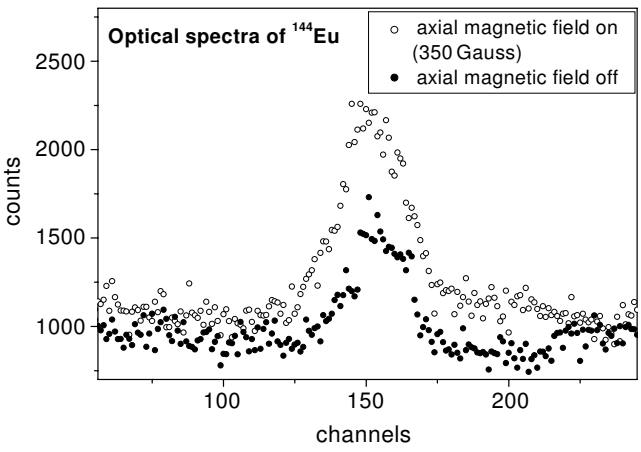

Fig. 5. Optical spectra of ^{144}Eu with and without magnetic field.

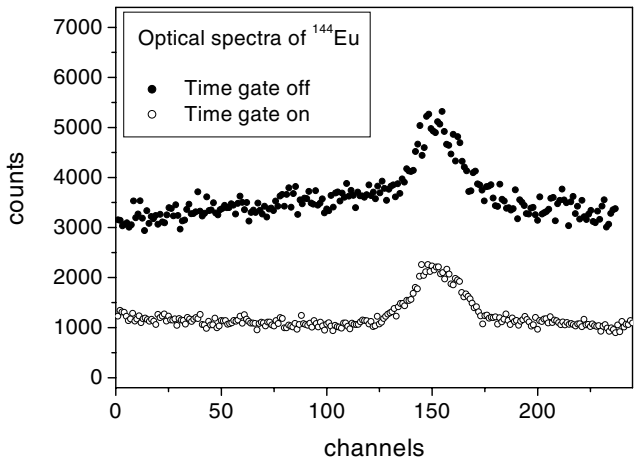

Fig. 6. Experimental optical spectra of ^{144}Eu obtained with time gate off and on.

800 gauss was applied (see fig. 4). The rise of resonance ionization efficiency was also observed for on-line produced Eu radioactive isotopes. In fig. 5 the optical spectra of ^{144}Eu with and without axial magnetic field are presented.

The selectivity (*i.e.* the ratio of the photoproduced ions to the background of surface-ionized ions) increases from 0.75 to 1.0, while the efficiency rises nearly twofold when the magnetic field is switched on. Any broadening or shift of the resonance for the stable Eu isotopes due to the magnetic field applied was not observed within the statistical error.

2.2.2 Time gate application for the selectivity rise

Due to the relatively low ionization potential of Eu (5.67 eV), an unwanted ionization of atoms on the hot surfaces of the laser ion source and target material occurs with high efficiency (up to 10%). Under these conditions the selectivity becomes a crucial factor for the applicability of the method. Surface-ionized ions are produced continously in time. The photoions are bunched and appear as an ion pulse with a duration of 35 μs rising 35 μs after interaction with the laser light. This bunching is caused by the heating voltage drop (of about 3 V) along the ion source tube. To improve the selectivity, the time gate method [11,12] has been used for on-line measurements of the isotope shifts of $^{144-137}$Eu. Rectangular electric impulses with amplitude equal to 60 V and duration equal to 35 μs (synchronized with the laser pulses) were applied to the deflector after the mass separator magnet (fig. 1). This leads to an increase of the selectivity from 0.4 to 1.0 (see fig. 6).

3 Experimental results

Isotope shifts for the chain of europium isotopes have been measured. For ^{142m}Eu, the γ line with energy 556.6 keV was used to avoid the influence of the short-lived ground state ($T_{1/2} = 2.4$ s). Examples of the experimental spectra obtained are shown in fig. 7.

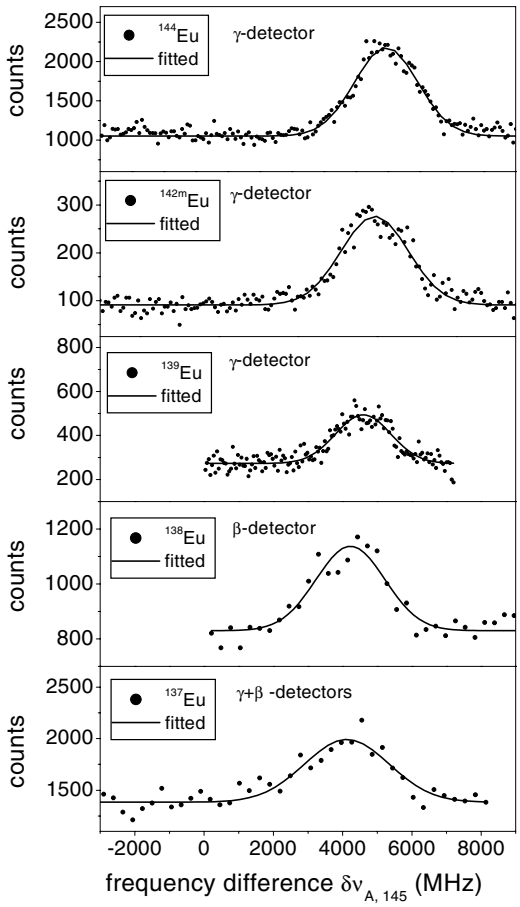

Fig. 7. Examples of the experimental spectra of ^{144,142m,139,138,137}Eu. The detectors for observing the radioactive ions are indicated.

Table 1 presents the experimental results of the isotope shifts measurements for neutron-deficient Eu isotopes. The results previously obtained by the conventional resonance ionization technique [13] are also shown. They are consistent with the new results within the experimental errors. This consistency additionally confirms the negligible influence of the magnetic field on the position of the centre of gravity of the observed lines. To extract the parameter $\lambda_{145,A}$ which is connected with the changes of the mean square charge radii $\delta\langle r^2\rangle_{145,A}$, the standard procedure [14] was used (with the electronic factor $F = -6.55$ GHz/fm^2 [14]). The specific mass shift for this pure s^2-sp transition was neglected [14]. The errors for $\lambda_{145,A}$ in table 1 are pure statistical; the uncertainty of the electronic factor is assumed to be about 5% [14]. In table 1 the values of $\lambda_{145,A}$ for $A = 141$–144 from [1] are also presented for comparison. They are based on the isotope shift measurements for the different optical lines (462.7 nm and 459.4 nm).

Table 1. Experimental results for isotope shifts in the 576.520 nm line of Eu isotopes. Nuclear parameter λ for $^{137-139,141,142m,143,144}$Eu is compared with parameter λ for ^{141,142m,143,144}Eu taken from ref. [1].

Isotope	$\Delta\nu_{145,A}$ (MHz)	$\Delta\nu_{145,A}$ (MHz), ref. [13]	$\lambda_{145,A}$ (fm^2)	$\lambda_{145,A}$ (fm^2), ref. [1]
^{144}Eu	240(160)	340(200)	−0.039(24)	−0.048(6)
^{143}Eu	150(160)	200(170)	−0.027(24)	−0.026(5)
^{142m}Eu	20(180)	35(150)	−0.009(27)	0.001(6)
^{141}Eu	−260(160)	−300(150)	0.031(24)	0.031(9)
^{139}Eu	−590(240)	−750(200)	0.079(37)	–
^{138}Eu	−880(220)	−500(350)	0.114(34)	–
^{137}Eu	−730(280)	–	0.096(44)	–

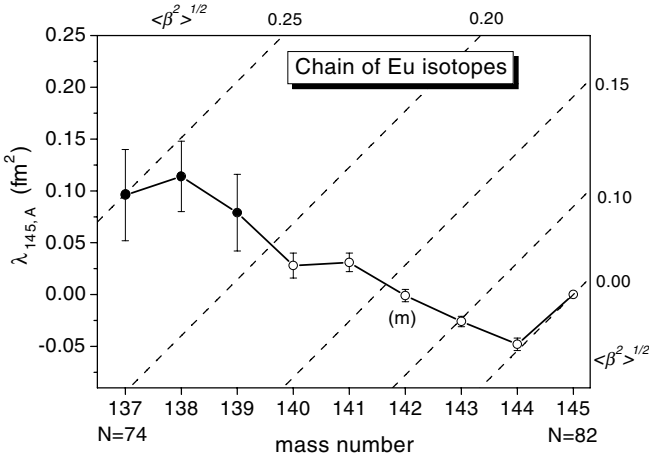

Fig. 8. Isotopic dependence of the $\lambda_{145,A}$ for Eu isotopes with $N < 82$. Data for $^{140-144}$Eu were taken from ref. [1].

4 Discussion

In fig. 8 the results of the $\lambda_{145,A} \approx \delta\langle r^2\rangle_{145,A}$ measurements for Eu isotopes are shown. The dashed lines of constant deformation have been obtained by using the standard two-parameter formula [14]:

$$\lambda_{145,A} = (1+x)\delta\langle r^2\rangle^{\rm DM}_{145,A} + y\frac{5}{4\pi}\langle r^2\rangle^{\rm DM}\delta\langle\beta^2\rangle_{145,A}\,,$$

where $x = \frac{C_2}{C_1}\frac{10}{7}R^2 + \frac{C_3}{C_1}\frac{5}{3}R^4$, $y = \frac{C_2}{C_1}2R^2 + \frac{C_3}{C_1}3R^4$, ($C_k$ are Seltzer coefficients [15] and $R = 1.2A^{1/3}$ fm), β is the quadrupole deformation and $\delta\langle r^2\rangle^{\rm DM}_{145,A}$ are calculated according to the Droplet Model [16]. We suppose that $\langle\beta^2\rangle = 0$ for the nucleus ^{145}Eu with magic neutron number $N = 82$ [1]. This assumption leads to a fair agreement of the deformations extracted from the isotope shifts data and the deformations calculated from the quadrupole moments for the strongly deformed Eu nuclei with $N > 88$. In table 2 the values of the quadrupole deformation parameters calculated by use of this formula are presented. Only $^{137-141}$Eu isotopes are included in this table because only for nuclei with relatively large mean squared deformation ($\sqrt{\langle\beta^2\rangle} > 0.15$) the comparison with the theoretical static deformation calculation are supposed to be reliable. For ^{141,140}Eu the more accurate data for $\lambda_{145,A}$ from [1] were used. The theoretical predictions for the deformation in the framework of the microscopic-macroscopic model [17] are also shown in table 2. The deformation parameter ε taken from [17] is recalculated to the β-parameter by the formula

$$\beta = \sqrt{\frac{\pi}{5}}\cdot\left(\frac{4}{3}\varepsilon + \frac{10}{63}\varepsilon^2\right)\,.$$

Table 2. Nuclear parameters λ with ^{145}Eu as reference and deformation parameters for the neutron-deficient Eu isotopes (λ parameters for ^{140,141}Eu were taken from ref. [1]).

Isotope	$\lambda \approx \delta\langle r^2\rangle$ (fm^2)	$\langle\beta^2_{\rm exp}\rangle^{1/2}$	$\beta_{\rm theor}$, ref. [17]
^{141}Eu	0.031(9)	0.173(3)	0.162
^{140}Eu	0.028(12)	0.190(3)	0.184
^{139}Eu	0.079(37)	0.221(10)	0.214
^{138}Eu	0.114(34)	0.246(8)	0.222
^{137}Eu	0.096(44)	0.253(10)	0.297

One can notice the rather good agreement of the theoretical and experimental values of β for $^{138-141}$Eu. However, the calculation overestimated the deformation of ^{137}Eu. For the predicted deformation parameters one has to observe a jump in the isotopic shift between ^{138}Eu and ^{137}Eu, which would be about −1700 MHz. Instead of the predicted jump-like deformation behaviour for the Eu nuclei with $N < 82$ one observes a gradual increase of deformation up to the value $\beta = 0.25$ for ^{137}Eu. The same conclusion was drawn in [18] from the comparison of the decoupled bands in ^{137,139}Eu. This gradual transition from the spherical nuclear shape near the magic neutron number $N = 82$ to a deformed one near $N = 74$ contrasted with the abrupt increase of deformation on the other side of the closed shell for Eu isotopes with $N > 89$. This different behaviour is considered to be connected with the different influence of the semi-magic number $Z = 64$ on the deformation development for nuclei with $N > 82$ and $N < 82$ [19]. A similar gradual increase of the deformation was observed previously for the adjacent ^{136,138}Sm isotopes [20,21]. The similarity of the bands in ^{137}Eu and ^{136}Sm points to the coincidence of the corresponding deformations [18]. According to [20,21] the deformation of ^{136}Sm is equal to $\beta = 0.25(1)$ and therefore it does coincide with the present estimation of the deformation of

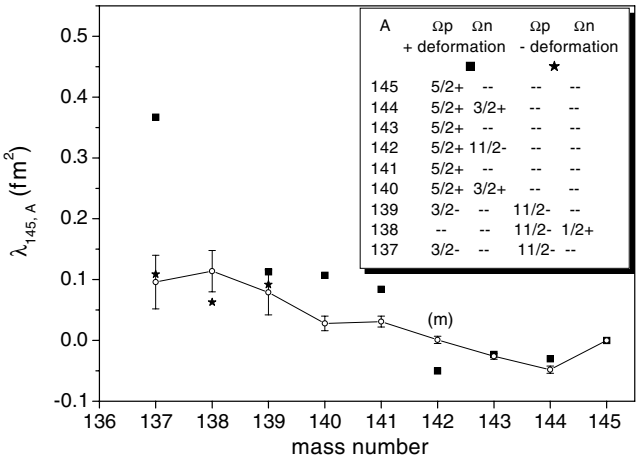

Fig. 9. Comparison of the $\lambda_{145,A}$ experimental dependence and Hartree-Fock calculations with SkM′ forces for the neutron-deficient Eu isotopes.

^{137}Eu from the isotope shift measurement (see table 2). On the other hand, the deformation of ^{136}Sm measured in [22] is markedly higher: $\beta = 0.30(1)$. To resolve this discrepancy the isotope shift of ^{136}Sm should be measured.

Hartree-Fock calculations with SkM′ forces for axially deformed nuclei (see the detailed description in [4]) have been performed for neutron-deficient Eu isotopes. The states blocked by the last odd particle were fixed in accordance with the known spin and parity of the corresponding nuclei (see table in fig. 9). For ^{137}Eu the agreement of the experimental and theoretical data can be obtained only for the negative deformation minimum, on condition that the proton state with $\Omega^\pi = 11/2^-$, which lies closest to the Fermi level, is blocked by the odd proton. Otherwise (see fig. 9) the same jump of deformation arises as in the microscopic-macroscopic calculations [17]. Thus the results of the Hartree-Fock calculations for the very neutron-deficient Eu nuclei are crucially dependent on the odd-particle states. It should be noted that for the proper theoretical description of ^{137,138,139}Eu a triaxial deformation should be taken into account [18] instead of the negative quadrupole deformation.

References

1. S.A. Ahmad *et al.*, Z. Phys. A **321**, 35 (1985).
2. G.D. Alkhazov *et al.*, JETP Lett. **37**, 274 (1983).
3. H.-J. Kluge, W. Nörtershäuser, Spectrochim. Acta B **58**, 1031 (2003).
4. G.D. Alkhazov *et al.*, Nucl. Phys. A **477**, 37 (1988).
5. G.D. Alkhazov *et al.*, Nucl. Instrum. Methods B **69**, 517 (1992).
6. A.E. Barzakh *et al.*, Phys. Rev. C **61**, 034304 (2000).
7. G.J. Zaal *et al.*, Z. Phys. A **290**, 339 (1979).
8. G.D. Alkhazov *et al.*, Nucl. Instrum. Methods A **280**, 141 (1989).
9. V.N. Panteleev *et al.*, Nucl. Instrum. Methods B **204**, 382 (2003).
10. V.N. Panteleev *et al.*, PNPI Preprint # 2511, 1 – 13 (2003).
11. Y. Jading *et al.*, Nucl. Instrum. Methods B **126**, 76 (1997).
12. A.E. Barzakh *et al.*, Nucl. Instrum. Methods B **126**, 85 (1997).
13. V.S. Letokhov *et al.*, J. Phys. G **18**, 1177 (1992).
14. E.W. Otten, *Treatise on Heavy-Ion Science*, edited by D.A. Bromley, Vol. **8** (Plenum Publishing, New York, 1989).
15. E.C. Seltzer, Phys. Rev. **188**, 1916 (1969).
16. W.D. Myers, K.-H. Schmidt, Nucl. Phys. A **410**, 61 (1983).
17. G.A. Leander, P. Moeller, Phys. Lett. B **110**, 17 (1982).
18. L. Goettig *et al.*, Nucl. Phys. A **475**, 569 (1987)
19. J.A. Cizewsky, E. Gulmez, Phys. Lett. B **175**, 11 (1986).
20. R. Wadsworth *et al.*, J. Phys. G **13**, 205 (1987).
21. A. Makishima *et al.*, Phys. Rev. C **34**, 576 (1986).
22. S. Lunardi *et al.*, Phys. Rev. C **38**, 537 (1988).